An Inductive-Power-Transfer Converter With High Efficiency Throughout Battery-Charging Process

Zhicong Huang, *Member, IEEE*, Siu-Chung Wong, *Senior Member, IEEE*, and Chi K. Tse, *Fellow, IEEE*

***Abstract*—An inductive power transfer (IPT) converter usually has an optimum efficiency only at a matched load. Because of wide load range variation during battery charging, it is challenging for an IPT converter to achieve the required output and maintain high efficiency throughout the charging process. In this paper, a series–series compensated IPT converter with an active rectifier is analyzed and implemented for battery charging. Appropriate operations are employed for constant-current charging and constant-voltage (CV) charging. A novel operation approach is proposed to achieve constant output voltage and to ensure load impedance matching during CV charging without the help of an extra dc–dc converter, which incurs loss. Both a frequency modulated primary inverter and a phase-angle modulated secondary active rectifier can achieve soft switching. High efficiency can be maintained during the whole battery-charging profile.**

***Index Terms*—Battery charging, efficiency optimization, inductive power transfer (IPT), soft switching.**

I. Introduction

AN INDUCTIVE power transfer (IPT) system can transfer power wirelessly from a transmitter coil to a receiver coil over a short-range air gap, which eliminates physical electrical contact between subsystems of the transmitter and the receiver with minimal electromagnetic radiation [1]. With such a wireless convenience, IPT has been used for battery charging in many applications, such as consumer electronics, biomedical implants, and electric vehicles [2]. Fig. 1 shows a typical charging profile of a battery, where the battery is charged initially by a constant current (CC) and subsequently by a constant voltage (CV) [3]. The charging process is started with CC charging at the rated value, where the battery voltage increases from the value of discharge cutoff to the value of charge threshold. The charging process is followed by CV charging at the charge threshold voltage to fully charge the battery, where the charging current decreases from the rated value to the minimum value at only a few percent of the rated value. The equivalent dc resistance of the battery increases significantly during the charging process.

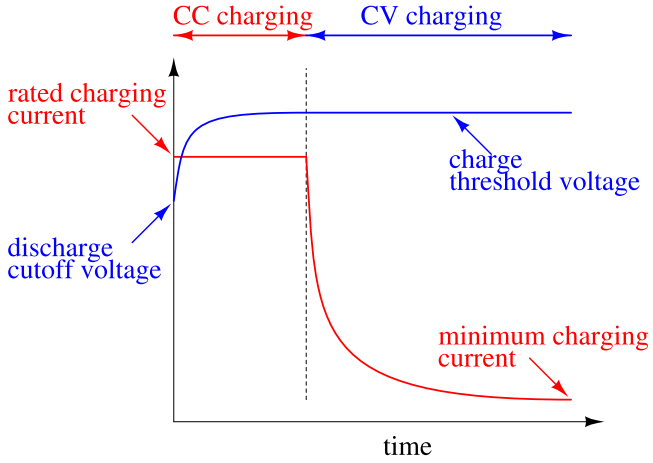

Fig. 1. Typical charging profile of a battery and operation modes of a battery charger.

Because of such a wide load range, efficiency optimization is a challenging design problem for most converters.

In an IPT system, the transmitter coil and the receiver coil form a loosely coupled transformer that has significant leakage inductances and a relatively small mutual inductance. Compensation of reactive power from the transformer using external reactive elements is often required to improve system performances, which may include power transfer capability, power efficiency, power regulation, and tolerance to misalignment between the coils [4]–[7]. The compensated transformer is often driven by an ac source generated from an inverter circuit for simplicity and good efficiency. An inverter circuit using half-bridge or full-bridge permits soft switching, which significantly improves efficiency. Soft switching can be designed to achieve zero-voltage switch-ON (ZVS) of metal-oxide-semiconductor field-effect transistor (MOSFET) switches or zero current switch-OFF of insulated-gate bipolar transistor (IGBT) switches. Phase-shift pulsewidth modulation (PWM) control can be used to modulate the input for the required output in battery charging. However, soft switching is hard to achieve even for a small modulation depth. In order for the inverter circuit to achieve soft switching at a fixed duty cycle, dc–dc converters at the front-side and/or the load-side are/is often incorporated in an IPT system to perform the required modulation of power. As a tradeoff, the maximum system efficiency suffers because of the use of more stages of power conversion. Alternatively, IPT converters can be designed at their native load-independent current (LIC) or load-independent voltage (LIV) output operating frequency [6],

Manuscript received July 27, 2018; revised November 7, 2018; accepted January 4, 2019. Date of publication January 9, 2019; date of current version June 28, 2019. This work was supported by Hong Kong Research Grants Council under General Research Grants 152082/17E and 152096/17E. Recommended for publication by Associate Editor O. C. Onar. *(Corresponding author: Zhicong Huang.)*

The authors are with the Department of Electronic and Information Engineering, Hong Kong Polytechnic University, Hong Kong (e-mail: zhicong.huang@connect.polyu.hk; enscwong@polyu.edu.hk; encktse@polyu.edu.hk).

Color versions of one or more of the figures in this paper are available online at http://ieeexplore.ieee.org.

Digital Object Identifier 10.1109/TPEL.2019.2891754

[8]–[11]. With the property of LIC or LIV, a very shallow duty-cycle modulation can provide precise charging at CC or CV operation. Therefore, a converter stage can be saved.

The battery-charging profile requires both CC and CV charging. Thus, a single IPT converter is designed with hybrid or switchable compensation topology to achieve both LIC and LIV outputs [12]–[14]. However, hybrid topologies need power switches in series with the power path; this incurs higher conduction loss and component cost. To reduce loss and cost, a single compensation topology can also be designed to operate at two operating frequencies both for the LIC and LIV outputs [15], [16].

The IPT converters mentioned above have the benefits of soft switching. They can be optimized both for CC and CV outputs with minimal control complexity. However, keeping the property of soft switching in mind, they cannot be optimized for the best efficiency using impedance matching without using a multistage design, which includes front-side and load-side dc–dc converters [18]–[23]. Because of the wide range of battery dc resistance during CV charging, we can say that without impedance matching, the efficiency of the IPT converter degrades significantly, as demonstrated in [12]–[16].

In multistage designs, the load-side dc–dc converter transforms the load impedance into matching load impedance to maintain the maximum efficiency, while the front-end dc–dc converter modulates the input voltage amplitude of the IPT converter to control the input power. The IPT converter is always kept at the optimal load and with soft switching. A wireless data feedback channel is normally required for the regulation of the output power. Different control schemes are studied, which include the minimum input current tracking [18], the maximum efficiency tracking [19]–[22], and the voltage ratio control [23]. The designs in [18] and [23] use a receiver-side dc–dc converter for the direct control of output power such that fast wireless communication between the transmitter and the receiver is not necessary. These *multistage* IPT systems with impedance matching for the maximum system efficiency have obvious drawbacks. Losses and costs of additional dc–dc converters are inevitable. More complicated controllers are needed for the whole system and the additional dc–dc converters.

The additional dc–dc converters in *multistage* IPT systems apply modulation to achieve impedance matching to maintain the system at the optimal efficiency point without losing the soft-switching property of the inverter. Alternatively, the modulation given by the additional dc–dc converter can be implemented by the inverter and the active rectifier circuit as shown in Fig. 2. Thus, the extra dc–dc converters can be omitted. However, it has been shown directly in [15] and indirectly in [12]–[16] that deep PWM of the inverter suffers high loss because of hard switching. Nevertheless, disregarding switching losses from the inverter bridge and the active rectifier, impedance matching has been implemented in [24] and [25]. In [24], [25], the modulation in the active rectifier ensures that the fundamental component of v_s and i_s are in phase, thus permitting direct application of the usual model for performing fundamental frequency analysis.

Without the implementation of impedance matching for efficiency optimization for wide load range, soft switching of the active rectifier bridge is demonstrated in [26] and [27]. A summary of desirable features for an IPT battery charger developed so far is presented in Table I. It will be desirable to develop an IPT battery charger that has an optimized efficiency for wide load range applications in CV charging, soft switching of the inverter and the active rectifier circuits, no extra dc–dc converter, no extra power switch, design for the battery charging profile, and receiver-side master control without the use of a fast wireless communication channel between the transmitter and the receiver.

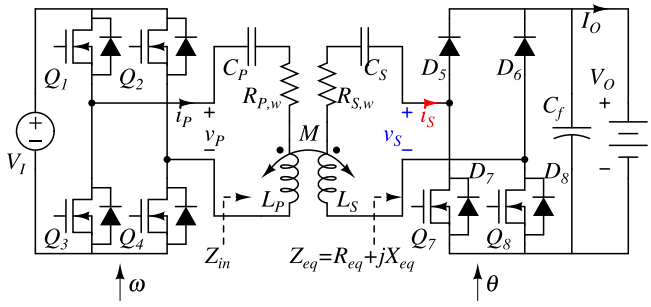

Fig. 2. Series–series IPT (SSIPT) system.

In this paper, we will develop an IPT battery charger as shown in Fig. 2 with all the desirable features in Table I. This paper is organized as follows. Section II highlights the system structure for battery charging and analyzes load impedance, voltage transfer ratio, efficiency, and input impedance of the SSIPT converter with the active rectifier. Section III defines critical criteria to achieve the maximum efficiency for an arbitrary operating frequency, and also defines a generally applicable load matching range for maintaining high system efficiency. Section IV proposes a novel approach to CV charging by controlling the operating frequency of the inverter and the conduction angle of the active rectifier. Section V experimentally verifies the output performance and efficiency performance. Finally, Section VI concludes this paper.

II. System Structure and Theoretical Analysis

A. System Structure

In the schematic of an SSIPT converter shown in Fig. 2, the magnetic coupler has self-inductances L_P and L_S, and mutual inductance M. Subscripts P and S indicate parameters in the primary and the secondary sides, respectively. The coupling coefficient is given by $k = \frac{M}{\sqrt{L_P L_S}}$. Both coils of the magnetic coupler are compensated by external capacitors C_P and C_S connected in series, with the resonant angular frequencies:

$$\omega_P = \frac{1}{\sqrt{L_P C_P}}, \text{and} \tag{1}$$

$$\omega_S = \frac{1}{\sqrt{L_S C_S}}. \tag{2}$$

Coil losses are represented by resistances $R_{P,w}$ and $R_{S,w}$. DC voltage source, V_I, is modulated to a high-frequency ac voltage, v_P, which drives the primary coil through a full-bridge inverter having four MOSFETs, Q_1–Q_4. The ac output is rectified to a dc output to charge the battery by an active rectifier with output filter capacitor, C_f. Secondary ac voltage, v_S, and secondary

TABLE I
DESIRABLE FEATURES OF AN IPT BATTERY CHARGER

Desirable feature	[12]–[14]	[15], [16]	[18], [23]	[19]–[22]	[24], [25]	[26], [27]
Efficiency optimization for wide load range	×	×	√	√	√	×
Soft switching of inverter and active rectifier circuits	√	√	√	√	×	√
No extra DC-DC converter	√	√	×	×	√	√
No extra power switch	×	√	√	√	√	√
Design for battery charging profile	√	√	√	√	√	×
Receiver side direct control	×	×	√	×	√	√

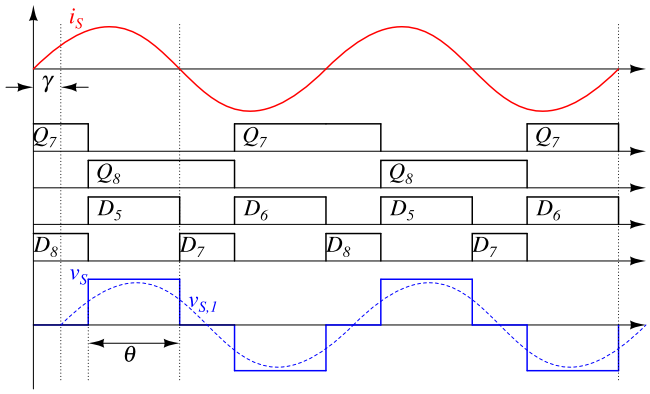

Fig. 3. Operation waveforms of the active rectifier.

ac current, i_S, are the inputs of the active rectifier circuit. DC voltage V_O and dc current I_O are charging the battery. The active rectifier consists of two MOSFETs, Q_7 and Q_8, and two diodes, D_5 and D_6. Also, D_7 and D_8 are the anti-parallel diodes of Q_7 and Q_8.

B. Operating Waveforms and Equivalent Model

The operating waveforms of the active rectifier are shown in Fig. 3. Transistors Q_7 and Q_8 are turned ON during the turn-on time of their anti-parallel diodes in order to achieve ZVS. Both Q_7 and Q_8 are turned ON for half a cycle. Therefore, Q_7 and Q_8 are turned OFF with a time delay of $\pi - \theta \in [0, \pi]$, until reaching the zero-cross points of i_S. Thus, conduction angle θ of the active rectifier varies between 0 and π. It should be noted that change in θ will affect the phase angle between v_S and i_S. As shown in Fig. 3, $v_{S,1}$ is the fundamental component of v_S, and it lags behind i_S with a phase angle given by $\gamma = \frac{\pi - \theta}{2}$. Therefore, the equivalent load is an impedance instead of the usual pure resistance.

Because the battery-charging process is slow compared to the operating period of the SSIPT converter, the battery can be modeled as a resistor determined by the charging voltage and the charging current, i.e., $R_L = \frac{V_O}{I_O}$. It has been studied that the active rectifier, together with resistive load, can be represented by an equivalent fundamental impedance [26], [27], given by

$$Z_{\text{eq}} = R_{\text{eq}} + jX_{\text{eq}} \tag{3}$$

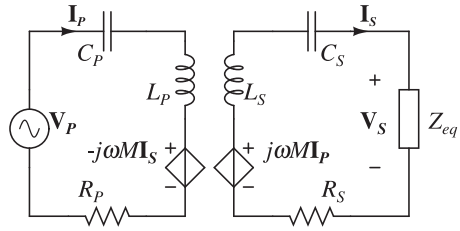

Fig. 4. AC equivalent circuit model of the SSIPT converter.

where

$$R_{\text{eq}} = \frac{8}{\pi^2} R_L \sin^4\left(\frac{\theta}{2}\right), \text{and} \tag{4}$$

$$X_{\text{eq}} = -\frac{8}{\pi^2} R_L \sin^3\left(\frac{\theta}{2}\right) \cos\left(\frac{\theta}{2}\right) \tag{5}$$

are equivalent resistance and reactance, respectively.

Fig. 4 shows an equivalent model of the SSIPT converter using fundamental approximation. This model is sufficiently accurate for high-quality resonant circuits operating near the resonant frequency. Here, $\mathbf{V}_P$, $\mathbf{I}_P$, $\mathbf{V}_S$, and $\mathbf{I}_S$ are phasors of the fundamental components of v_P, i_P, v_S, and i_S, respectively. Resistor R_P includes losses from the primary coil and the inverter, while resistor R_S includes losses from the secondary coil and the active rectifier. The load is represented by an equivalent impedance, Z_{eq}, with resistance R_{eq} and reactance X_{eq}.

The basic equations for the circuit model in Fig. 4 are

$$(R_P + jX_P)\mathbf{I_P} - jX_M\mathbf{I}_S = \mathbf{V}_P \tag{6}$$

$$-(R_S + R_{\text{eq}} + jX_S)\mathbf{I}_S + jX_M\mathbf{I}_P = 0 \tag{7}$$

where

$$X_M = \omega M \tag{8}$$

$$X_P = \omega L_P - \frac{1}{\omega C_P}, \text{and} \tag{9}$$

$$X_S = \omega L_S - \frac{1}{\omega C_S} + X_{\text{eq}} \tag{10}$$

are mutual reactance, transmitter-side reactance, and receiver-side reactance, respectively. The operating angular frequency is represented by ω. The input voltage of the active rectifier is given by $\mathbf{V}_S = (R_{\text{eq}} + jX_{\text{eq}})\mathbf{I}_S$.

C. Voltage Transfer Ratio, Power Efficiency, and Input Impedance

Using Fourier analysis, the magnitudes of $\mathbf{V}_P$ and $\mathbf{V}_S$ are given by

$$|\mathbf{V}_P| = \frac{4}{\pi} V_I, \text{and} \tag{11}$$

$$|\mathbf{V}_S| = \frac{4}{\pi} \sin\left(\frac{\theta}{2}\right) V_O. \tag{12}$$

From (6)–(12), the dc voltage transfer ratio of the SSIPT converter shown in Fig. 2 can be calculated as

$$G_V = \frac{V_O}{V_I} \tag{13}$$

$$= \left| \frac{X_M \frac{Z_{\text{eq}}}{\sin(\frac{\theta}{2})}}{(R_P + jX_P)(R_S + R_{\text{eq}} + jX_S) + X_M^2} \right|. \tag{14}$$

Using the equivalent model shown in Fig. 4, the efficiency

$$\eta = \frac{|\mathbf{I}|_S^2 R_{\text{eq}}}{|\mathbf{I}|_S^2 R_{\text{eq}} + |\mathbf{I}|_S^2 R_S + |\mathbf{I}|_P^2 R_P} \tag{15}$$

$$= \frac{X_M^2 R_{\text{eq}}}{[(R_{\text{eq}} + R_S)^2 + X_S^2] R_P + X_M^2 (R_{\text{eq}} + R_S)}. \tag{16}$$

The input impedance and input phase angle are, respectively,

$$Z_{\text{in}} = R_P + jX_P + \frac{X_M^2}{R_{\text{eq}} + R_S + jX_S}, \text{and} \tag{17}$$

$$\varphi = \frac{180}{\pi} \arctan \frac{\Re(Z_{\text{in}})}{\Im(Z_{\text{in}})} \tag{18}$$

where $\Re(Z_{\text{in}})$ and $\Im(Z_{\text{in}})$ are the real and imaginary components of the input impedance, Z_{in}, respectively.

III. Efficiency Optimization

A. Theoretical Maximum Efficiency

The power efficiency given in (16) can be simplified as

$$\eta \approx \frac{1}{\frac{R_{\text{eq}} + \frac{X_S^2}{R_{\text{eq}}}}{X_M^2} R_P + \frac{R_S}{R_{\text{eq}}} + 1} \tag{19}$$

with assumptions $\frac{X_M^2}{R_P R_S} \gg 1$ and $\frac{R_{\text{eq}}}{R_S} > 1$.

We will find the optimum values of R_{eq} and X_{eq} leading to maximum efficiency. For an arbitrary operating frequency, ω, from (19), it is obvious that the efficiency can be maximized as

$$\eta_{\text{opt}} \approx \frac{1}{\frac{1}{k\sqrt{Q_P Q_S}} + 1}, \text{if} \tag{20}$$

$$X_{S,\text{opt}} = \omega L_S - \frac{1}{\omega C_S} + X_{\text{eq}} = 0, \text{and} \tag{21}$$

$$R_{\text{eq,opt}} = \omega M \sqrt{\frac{R_S}{R_P}} \tag{22}$$

where $Q_P = \frac{\omega L_P}{R_P}$ and $Q_S = \frac{\omega L_S}{R_S}$ are quality factors of the primary and secondary sides, respectively.

TABLE II
Simulation Parameters of the SSIPT Converter for Analysis

Parameters	Symbols	Values
Self inductance	L_P, L_S	118 μH, 172 μH
Coupling coefficient	k	0.283
Equivalent Resistance	R_P, R_S	0.5 mΩ, 0.72 mΩ
Compensation capacitance	C_P, C_S	85.865 nF, 58.908 nF
Resonant frequency	$\frac{\omega_P}{2\pi} = \frac{\omega_S}{2\pi}$	50 kHz

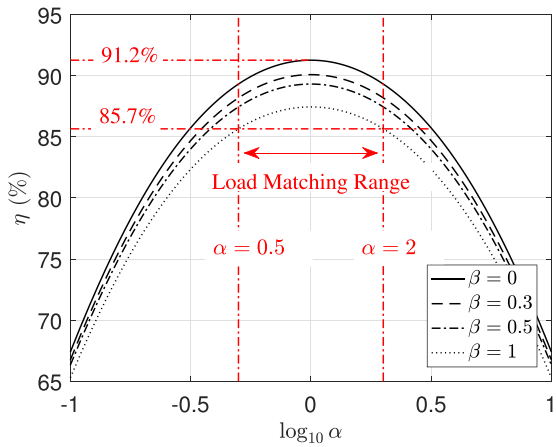

Fig. 5. Efficiency of the SSIPT converter versus $\log_{10} \alpha$.

Equations (21) and (22) are the criteria of critical load impedance matching point that achieves the maximum efficiency for an arbitrary operating frequency, ω. Maximum efficiency, η_{opt}, in (20) is frequency dependent. For near constant values of R_P and R_S within a certain range of operating frequency, it is possible to achieve a higher efficiency as operating frequency, ω, increases, due to higher Q_P and Q_S.

B. Load Impedance Matching Range for Efficiency Optimization

Because the modulation of the active rectifier given in Fig. 3 cannot alter R_{eq} and X_{eq} independently, it is impractical for the SSIPT converter to operate exactly at $R_{\text{eq,opt}}$ and $X_{S,\text{opt}}$ in order to achieve the maximum efficiency. We will find a range of R_{eq} and X_{eq}, which gives acceptable efficiency performance. In doing so, we define a factor, α, representing normalized R_{eq} with respect to $R_{\text{eq,opt}}$, i.e.,

$$\alpha = \frac{R_{\text{eq}}}{R_{\text{eq,opt}}} \tag{23}$$

and a factor, β, representing the deviation of the normalized X_{eq} from 0, i.e.,

$$\beta = \frac{\frac{X_S^2}{R_{\text{eq}}}}{R_{\text{eq,opt}}}. \tag{24}$$

As an illustration, the efficiency of an SSIPT converter using the parameters shown in Table II is plotted versus $\log_{10} \alpha$ at some values of $\beta < 1$ as shown in Fig. 5. A range of α and β can

TABLE III
OPERATION OF THE SSIPT CONVERTER

Charging process	Operating frequency ω	Conduction angle θ
CC	ω_P	π
CV	Adjust according to optimal points shown in Fig. 9.	

be selected for an acceptable minimum efficiency, say, 85.7%. Thus, $0.5 < \alpha < 2$ and $\beta < 1$ are selected. Unless specified otherwise, the parameters given in Table II will be used for the rest of this paper.

IV. Design for Battery Charging

A. CC Charging

It is well known that an SSIPT converter can achieve LIC for CC charging at a high-efficiency point [5], [10], [13], [15]. The design methodology of the SSIPT converter with constant output current has been studied in [15], [28]. Because the range of battery resistance in CC charging is usually narrow, therefore by locating the resistance range of CC charging within the load impedance matching range of the SSIPT converter, high efficiency can be achieved for CC charging, as shown by the red curve in Fig. 10(a). Precise output current is not necessary for CC charging. Therefore, the SSIPT converter can operate without any modulation, i.e., the active rectifier can operate similar to a passive rectifier with the following condition:

$$\theta_{\rm CC} = \pi \tag{25}$$

and the inverter can operate with high efficiency at a fixed frequency given by

$$\omega_{\rm CC} = \omega_P. \tag{26}$$

The operation of the SSIPT converter in CC charging is summarized in Table III.

Theoretically, if component losses are neglected, the output current is given by

$$I_O \approx \frac{8}{\pi^2}\frac{V_I}{\omega_P M}. \tag{27}$$

Substituting (22), (25), and (26) into (14), the output voltage at the load matching point can be obtained as

$$G_{V,\rm opt} \approx \sqrt{\frac{L_S}{L_P}} \tag{28}$$

provided that component losses are neglected, and the load quality factors in the primary and the secondary sides are identical, i.e., $\frac{\omega L_P}{R_P} = \frac{\omega L_S}{R_S}$.

It should be noted that if primary resonant frequency, ω_P, and secondary resonant frequency, ω_S, are identical, then input impedance, $Z_{\rm in}$, of the SSIPT converter is purely resistive. To provide a slightly inductive input impedance for operating the primary inverter at ZVS, ω_P can be slightly lower than ω_S [15], [28].

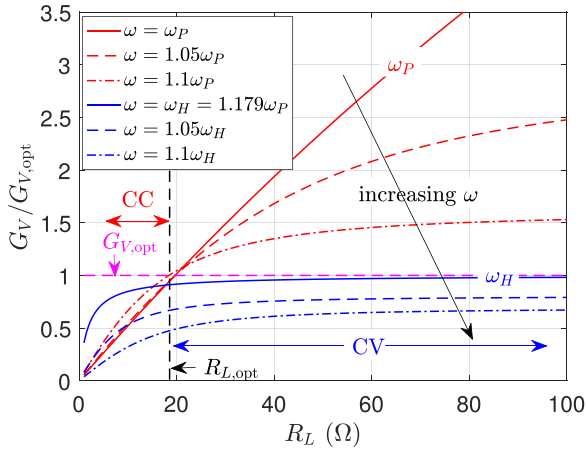

Fig. 6. Voltage transfer ratio versus load resistance under various operating frequencies.

B. CV Charging

For CV charging, a precisely regulated output voltage is needed to charge the battery. An extra over-voltage protection is usually implemented for safe operation. The efficiency of the SSIPT converter should also be optimized using impedance transformation for the wide load range of CV charging. For the SSIPT converter with the active rectifier shown in Fig. 2, we have two independent control parameters, which are as follows:

1) the operating frequency, ω, of the inverter;
2) the conduction angle, θ, of the active rectifier.

Although we can readily achieve CV output by controlling ω and θ, yet we first restrict the range of ω by considering over-voltage protection. The charging power will keep on increasing during CC charging until the battery voltage reaches the charge threshold value. At the point of reaching the maximum charging power, it is safer for the inverter to switch to another operating frequency, where over-voltage will not occur, even if there is no control in the secondary active rectifier. Fig. 6 shows the voltage transfer ratio versus load resistance under different operating frequencies. In CC charging, the SSIPT converter operates at ω_P to achieve a constant output current, as the solid red curve shows. In CV charging, if the operating frequency is more than ω_H, the voltage transfer ratio, G_V, will always be smaller than $G_{V,\rm opt}$, as shown by the solid blue curve and dashed magenta curve. Frequency $\omega_H = \frac{\omega_P}{\sqrt{1-k}}$ is the operating frequency of the SSIPT converter at which an LIV output is achieved [15]. Therefore, we can switch the operating frequency from ω_P to ω_H once the maximum charging power is reached for a safe charging operation. During CV charging, the control of ω will start from ω_H.

Because winding loss and converter loss are inevitable, practical voltage transfer ratio, G_V, will always be smaller than $G_{V,\rm opt} = \sqrt{\frac{L_S}{L_P}}$. Specifically, G_V is designed at $0.9\sqrt{\frac{L_S}{L_P}} \approx 1.09$ as an example. Fig. 7 shows the variation of voltage transfer ratio, G_V, versus operating frequency, ω, and conduction angle, θ, under different load conditions. The operating points $\{(\omega, \theta)\}$ for achieving $G_V = 1.09$ are plotted in three-dimensional (3-D) space as red curves shown in Fig. 7

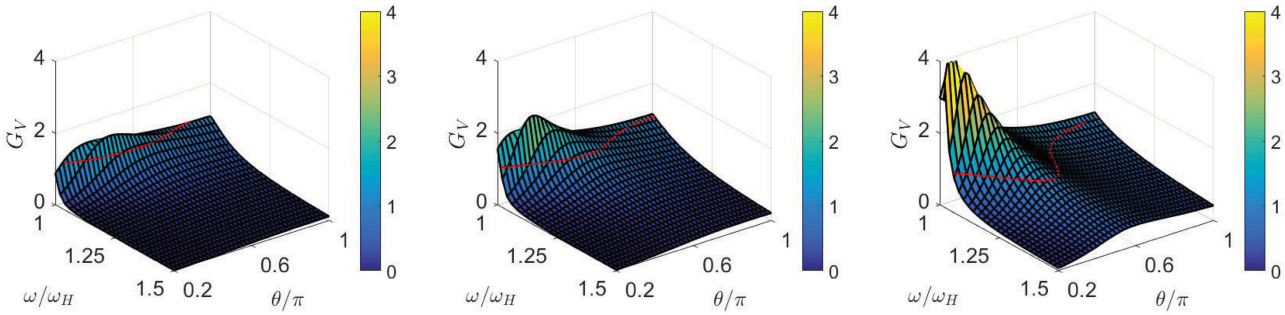

Fig. 7. Variation of voltage transfer ratio, G_V, with respect to operating frequency, ω, and conduction angle, θ, for (a) $R_L = 10\ \Omega$, (b) $R_L = 30\ \Omega$, and (c) $R_L = 100\ \Omega$.

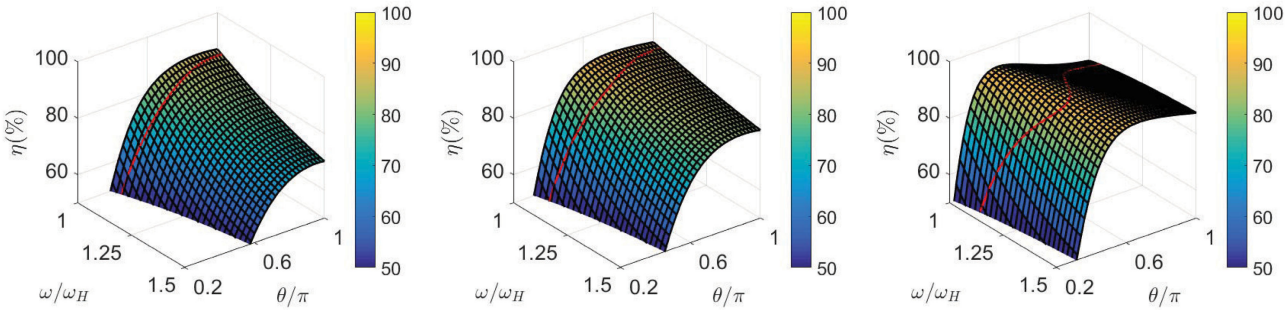

Fig. 8. Variation of efficiency η with respect to operating frequency, ω, and conduction angle, θ, for (a) $R_L = 10\ \Omega$, (b) $R_L = 30\ \Omega$, and (c) $R_L = 100\ \Omega$.

under different loading conditions. Fig. 8 shows the corresponding variation of efficiency η. Among operating points $\{(\omega, \theta)\}$, we can identify the locations in the load impedance matching range, as illustrated in Fig. 5, to achieve a constant output voltage with high efficiency.

Therefore, the following two-step procedure can be performed to derive the operating points for CV charging using a numerical calculation tool such as MATLAB.

1) Given a constant G_V, solve (14) to find all the solutions $A_i\{(\omega, \theta)\}$ for each load $R_{L,i}$ in CV charging, where $\omega > \omega_H$ and $0 < \theta < \pi$ are the constraints.
2) Substitute $A_i\{(\omega, \theta)\}$ into (16) and search for the maximum efficiency, and find the optimum operation points $A_i(\omega_{\rm CV}, \theta_{\rm CV})$ for each load $R_{L,i}$ in CV charging.

With these numerical solutions, the operating points in the load impedance matching range can be found to achieve CV output. Fig. 9 demonstrates the solution in a 2-D space. Solid curves in different colors represent possible solutions to achieve constant G_V for different load conditions. Points marked with "x" are the optimum operating points having the maximum efficiency, for R_L varying from 15 to 160 Ω as indicated by arrow direction.

Because battery charging is a slow process, the dynamic response is not a critical issue for efficiency optimization. It is feasible to implement the control with the optimum operating point set at (ω, θ), as shown in Fig. 9, using entries of R_L through lookup table. The SSIPT converter can achieve fast and precise control of constant output voltage by modulating θ in the receiver side for CV charging. To maintain high efficiency during the whole CV charging process, the information of loading resistance can be fed back to the transmitter side wirelessly for the control of ω.

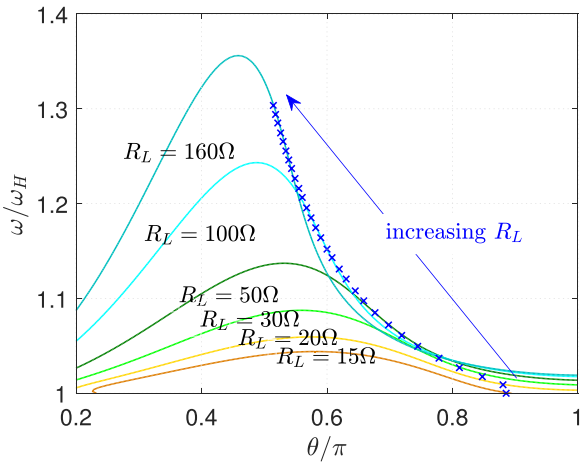

Fig. 9. Numerical solutions shown as a curve for some selected load resistances to achieve a constant $G_V = 1.09$, and the optimum operating points marked as "x" to have high efficiency.

C. Comparison of Efficiency and Load Impedance

Efficiency comparison between the SSIPT converter designed with the conventional approach in [15], which does not have

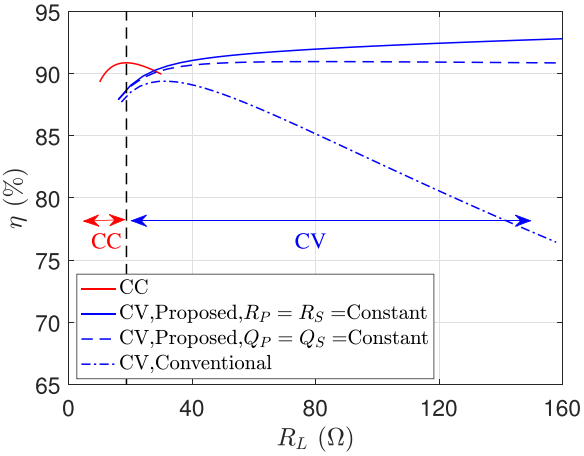

(a)

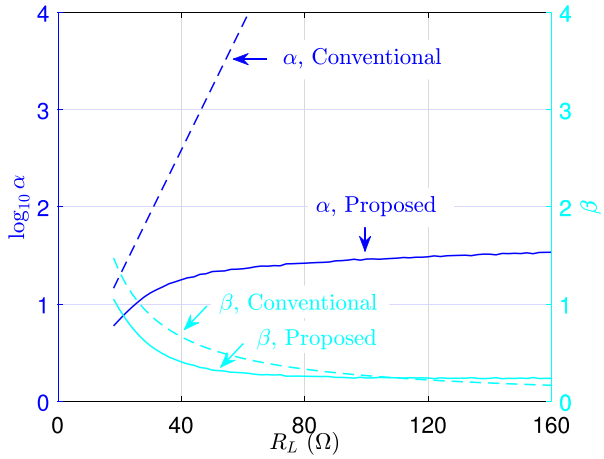

(b)

Fig. 10. Comparisons between the proposed approach in this paper and the conventional approach in [15] for (a) efficiency, and (b) α and β versus R_L.

efficiency optimization for the wide load range during CV charging, and the SSIPT converter developed in this paper will be presented in this section. As shown in Fig. 10(a), the efficiency degrades significantly as the battery resistance increases rapidly during CV charging, due to mismatch in the load impedance. On the basis of the proposed approach in Section IV-B, the novel SSIPT converter can achieve constant output voltage for CV charging, with the ability to transform load impedance within a matching range. The efficiency is kept high as shown by the blue solid curve or blue-dash curve in Fig. 10(a). The blue solid curve is obtained by simulation with constant resistances R_P and R_S, while the blue-dash-dot curve corresponds to constant quality factors, Q_P and Q_S.

As discussed in Section III-B, a load matching range can be defined by $0.5 < \alpha < 2$ and $\beta < 1$. From Fig. 10(b), it can be observed that the load impedance is located within a matching range while using the proposed approach, as the solid blue curve and the solid cyan curve show. However, as a comparison, the load resistance of the conventional approach deviates from the matching range significantly as shown by the blue dash curve in Fig. 10(b).

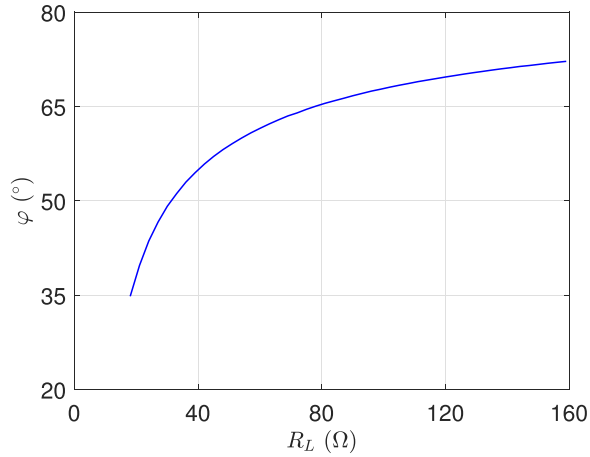

Fig. 11. Input phase angle of the SSIPT converter during CV charging process.

TABLE IV
CHARGING SPECIFICATIONS

Charging Specifications	Values
Discharge cut-off voltage	36 V
Charge threshold voltage	52 V
Rated charge current	3A
Minimum charge current	0.3A

D. Soft Switching

In CV charging, the operation of the secondary active rectifier can achieve ZVS as discussed in Section II-B. Substituting operating points $A_i(\omega_{\rm CV}, \theta_{\rm CV})$ into (17), the input impedance can be calculated. With (18), input phase angle φ is plotted in Fig. 11. Since φ is always positive, the primary inverter can always operate at ZVS during the whole CV charging process.

V. EXPERIMENTAL VERIFICATION

A. Experimental Prototype

To verify the efficiency performance of the proposed approach, an experimental prototype is built according to Fig. 2. According to the charging profile shown in Fig. 1 and its specifications given in Table IV, the battery resistance ranges from 12 to 17.3 Ω for CC charging and 17.3 to 173 Ω for CV charging. System parameters are presented in Table V. An electronic load is used to emulate the equivalent resistance of the battery.

B. Measured Operating Points, Efficiency, and Waveforms

First, the active rectifier operates as a passive rectifier, and the inverter operates at $\frac{\omega_P}{2\pi} = 49.98$ kHz to achieve native LIC for CC charging. Measured output current points (marked with "□") are shown in Fig. 13(a). It can be observed that the output current is nearly constant at 3 A, which satisfies the require-

TABLE V
SYSTEM PARAMETERS

System Parameters	Symbols	Values
Input voltage	V_I	50V
Switch	Q_1-Q_8, D_5-D_6	IPP60R165, MBR20200
Self inductance	L_P, L_S	117.6 μH, 172.7 μH
Coupling coefficient	k	0.283
Coil resistance	$R_{P,w}$, $R_{S,w}$	0.41 mΩ, 0.54 mΩ
Compensation capacitance	C_P, C_S	86.22 nF, 56.04 nF
Resonant frequency	$\frac{\omega_P}{2\pi}$, $\frac{\omega_S}{2\pi}$	49.98 kHz, 51.16 kHz

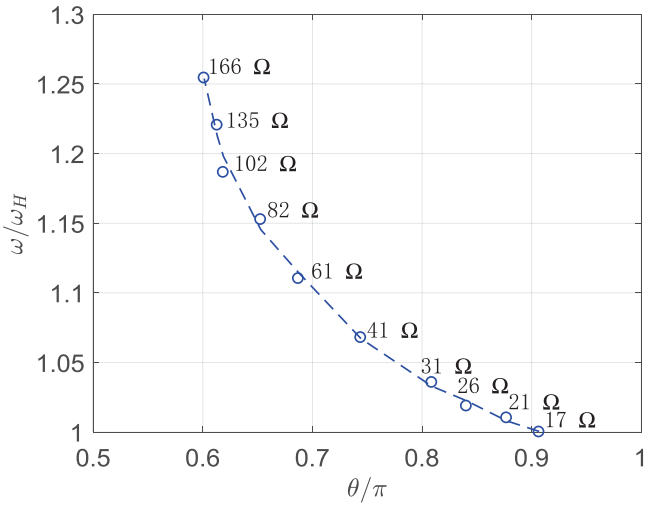

Fig. 12. Measured operating points at a fixed voltage output of 52 V and the corresponding load resistances.

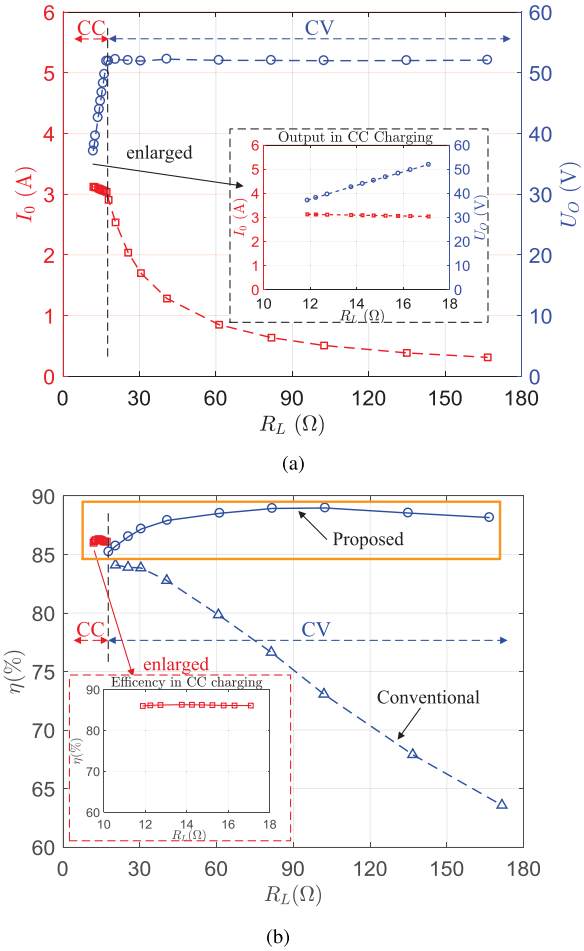

Fig. 13. (a) Measured output current and voltage versus battery resistance. (b) Measured efficiency versus battery resistance.

ment of CC charging. Second, after the battery voltage reaches 52 V, CV charging should be employed. Following the proposed operation approach in Section IV-B, conduction angle, θ, of the active rectifier and operating frequency, ω, of the inverter are adjusted to achieve CV output with the optimum efficiency performance. The measured operating points (marked with "◯") are shown in Fig. 12, with ω varying from 59 to 74 kHz and θ from 168° to 108°. The corresponding output voltages (marked with "◯") are kept at 52 V, as shown in Fig. 13(a). The output voltage satisfies the requirement of CV charging.

The input dc power and output dc power are measured using a precision power scope, Yokogawa PX8000. The measured efficiency points of the whole charging process are shown in Fig. 13, within the highlighted orange box. Efficiency points of CC charging (marked with "□") are approximately 86%. The measured efficiency points of CV charging (marked with "◯") are from 85% to 89%. As a comparison, the measured efficiency points (marked with "△") using the conventional approach [15] to achieve constant output voltage are also shown in Fig. 13, which decreases significantly as the battery resistance increases. To sum up, a high efficiency can be maintained for the whole charging process by using the proposed approach. The higher efficiency during CV charging than CC charging is attributed to the reduced conduction loss of using the active rectifier and the higher quality factors of the transformer coils at higher operating frequencies.

Waveforms of the inverter and the active rectifier at the start and end of CV charging are shown in Fig. 14(a) and (b), respectively. It can be observed that ZVS is achievable both in the inverter and the active rectifier. Efficiency measurements at the start and end of CV charging are shown in Fig. 15(a) and (b), respectively.

C. Transient Response Against Variations of Load and Input

The closed-loop control demonstrated in Section IV-B has been implemented for CV charging. Transient waveforms for step changing of load resistance and input voltage are shown in Fig. 16. The output voltage, V_O, and output current, I_O, are measured and shown as CH1 in dark blue and CH2 in light blue. The control variables are observed from digital-to-analog outputs, where CH3 in magenta and CH4 in green represent the conduction angle, θ, and operating frequency, ω, respectively. It can be observed that V_O is tightly regulated by the fast receiver-side direct control of θ. Slower control of ω in the transmitter side is based on the wireless feedback of the load information

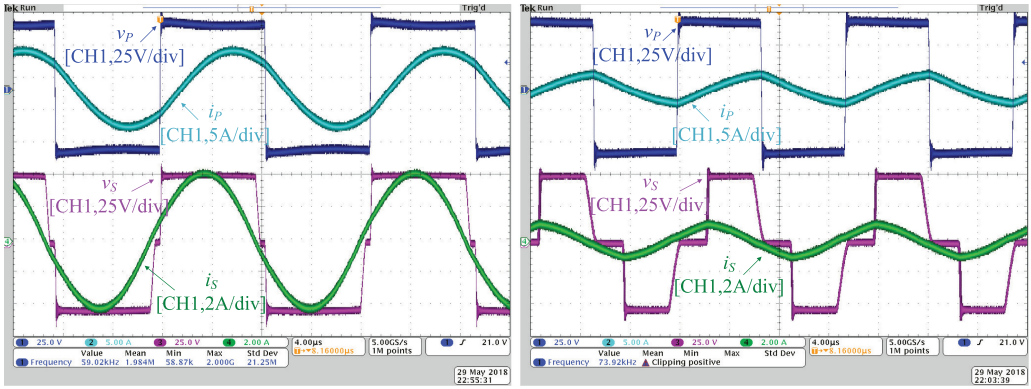

(a) (b)

Fig. 14. Waveforms of the inverter and the active rectifier circuits at (a) the start and (b) the end of CV charging.

(a)

(b)

Fig. 15. Screen capture of efficiency measurement at (a) the start and (b) the end of CV charging.

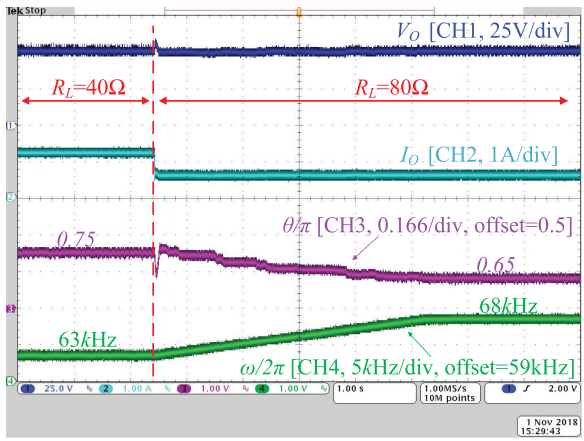

(a)

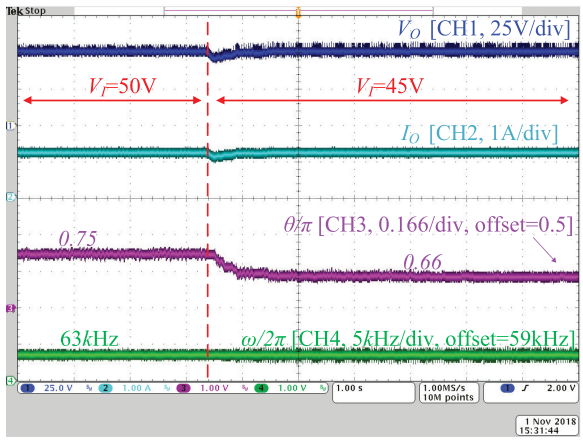

(b)

Fig. 16. Transient waveforms for (a) R_L step switching from 40 to 80 Ω, and (b) V_I step switching from 50 to 45 V, $R_L = 40\ \Omega$.

and the lookup table shown in Fig. 12, to locate the optimum operating point for high efficiency. Fig. 16(b) shows the transient waveforms when there is a step change of input voltage, V_I, from 50 to 45 V. Output voltage, V_O, can still be maintained by modulating θ. Because there is no load change, ω remains unchanged. Therefore, the SSIPT converter may shift slightly from its optimum operating point if there is fluctuation in the input voltage.

D. Discussion on Misalignment Issue

For stationary IPT applications of battery charging, the coupling coefficient is usually constant once the positioning process is finished. It will rarely fluctuate during the charging process. However, misalignment problem may occur because of low-

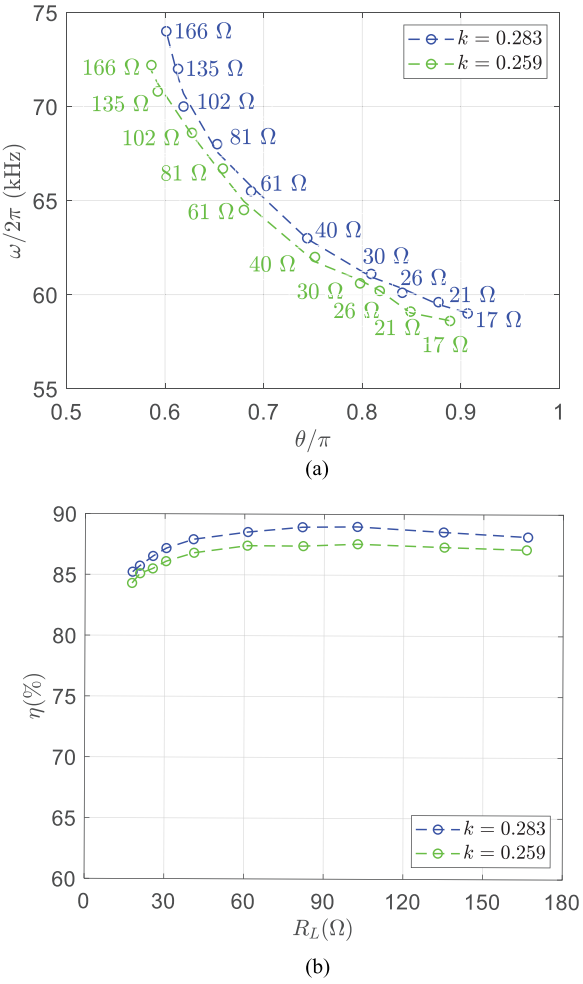

Fig. 17. (a) Measured operating points at a fixed voltage output of 52 V, and (b) measured efficiency versus load resistance, under $k = 0.283$ and $k = 0.259$.

precision positioning, which leads to small variation in the coupling coefficient. Some available solutions can be used to solve this misalignment problem. First, novel design of coil structure has been proposed to minimize the variation in the coupling coefficient due to misalignment to some acceptable levels [29]. Second, good alignment can be ensured using positioning systems with abilities of self-detection and auto-calibration [30]. Even if a small misalignment occurs in some practical applications, parameter identification methods of IPT systems can be used to acquire an accurate coupling coefficient [31]. Moreover, more sets of operating points under different values of the coupling coefficient can be measured and stored in the lookup table. Therefore, the closed-loop control against misalignment can still be realized to achieve constant output voltage and maintain high efficiency. For example, two sets of (ω, θ) under $k = 0.259$ and $k = 0.283$ are measured in Fig. 17(a), with their corresponding measured efficiency curves shown in Fig. 17(b).

VI. Conclusion

An SSIPT battery charger that permits efficiency optimization for a wide load range, soft switching of inverter, and active rectifier circuits, no extra dc–dc converter, no extra power switch, and receiver-side direct control, is analyzed and implemented in this paper. Different operations are employed for CC charging and CV charging. A novel operation approach is proposed to achieve constant output voltage and to ensure load impedance matching during CV charging, by controlling the operating frequency of the primary inverter and the conduction angle of the secondary active rectifier. High efficiency can be maintained for the whole battery charging process.

References

[1] S. Y. R. Hui, W. Zhong, and C. K. Lee, "A critical review of recent progress in mid-range wireless power transfer," *IEEE Trans. Power Electron.*, vol. 29, no. 9, pp. 4500–4511, Sep. 2014.

[2] G. A. Covic and J. T. Boys, "Inductive power transfer," *Proc. IEEE*, vol. 101, no. 6, pp. 1276–1289, Jun. 2013.

[3] A. A. Hussein and I. Batarseh, "A review of charging algorithms for nickel and lithium battery chargers," *IEEE Trans. Veh. Technol.*, vol. 60, no. 3, pp. 830–838, Mar. 2011.

[4] C. S. Wang, G. A. Covic, and O. H. Stielau, "Power transfer capability and bifurcation phenomena of loosely coupled inductive power transfer systems," *IEEE Trans. Ind. Electron.*, vol. 51, no. 1, pp. 148–157, Feb. 2004.

[5] Y. H. Sohn, B. H. Choi, E. S. Lee, G. C. Lim, G. H. Cho, and C. T. Rim, "General unified analyses of two-capacitor inductive power transfer systems: Equivalence of current-source SS and SP compensations," *IEEE Trans. Power Electron.*, vol. 30, no. 11, pp. 6030–6045, Nov. 2015.

[6] W. Zhang and C. C. Mi, "Compensation topologies of high-power wireless power transfer systems," *IEEE Trans. Veh. Technol.*, vol. 65, no. 6, pp. 4768–4778, Jun. 2016.

[7] J. L. Villa, J. Sallan, J. F. S. Osorio, and A. Llombart, "High-misalignment tolerant compensation topology for ICPT systems," *IEEE Trans. Ind. Electron.*, vol. 59, no. 2, pp. 945–951, Feb. 2012.

[8] W. Zhang, S. C. Wong, C. K. Tse, and Q. Chen, "Design for efficiency optimization and voltage controllability of series–series compensated inductive power transfer systems," *IEEE Trans. Power Electron.*, vol. 29, no. 1, pp. 191–200, Jan. 2014.

[9] W. Zhang, S. C. Wong, C. K. Tse, and Q. Chen, "Analysis and comparison of secondary series and parallel compensated inductive power transfer systems operating for optimal efficiency and load-independent voltage transfer ratio," *IEEE Trans. Power Electron.*, vol. 29, no. 6, pp. 2979–2990, Jun. 2014.

[10] W. Zhang, S. C. Wong, C. K. Tse, and Q. Chen, "Load-independent duality of current and voltage outputs of a series or parallel compensated inductive power transfer converter with optimized efficiency," *IEEE J. Emerg. Sel. Topics. Power Electron.*, vol. 3, no. 1, pp. 137–146, Mar. 2015.

[11] S. Samanta and A. K. Rathore, "Analysis and design of load-independent ZPA operation for P/S, PS/S, P/SP, and PS/SP tank networks in IPT applications," *IEEE Trans. Power Electron.*, vol. 33, no. 8, pp. 6476–6482, Aug. 2018.

[12] C. Auvigne, P. Germano, D. Ladas, and Y. Perriard, "A dual-topology ICPT applied to an electric vehicle battery charger," in *Proc. Int. Conf. Elect. Mach.*, Mar. 2012, pp. 2287–2292.

[13] X. Qu, H. Han, S. C. Wong, C. K. Tse, and W. Chen, "Hybrid IPT topologies with constant current or constant voltage output for battery charging applications," *IEEE Trans. Power Electron.*, vol. 30, no. 11, pp. 6329–6337, Nov. 2015.

[14] R. Mai, Y. Chen, Y. Li, Y. Zhang, G. Cao, and Z. He, "Inductive power transfer for massive electric bicycles charging based on hybrid topology switching with a single inverter," *IEEE Trans. Power Electron.*, vol. 32, no. 8, pp. 5897–5906, Aug. 2017.

[15] Z. Huang, S. C. Wong, and C. K. Tse, "Design of a single-stage inductive-power-transfer converter for efficient EV battery charging," *IEEE Trans. Veh. Technol.*, vol. 66, no. 7, pp. 5808–5821, Jul. 2017.

[16] V. B. Vu, D. H. Tran, and W. Choi, "Implementation of the constant current and constant voltage charge of inductive power transfer systems with the double-sided LCC compensation topology for electric vehicle battery charge applications," *IEEE Trans. Power Electron.*, vol. 33, no. 9, pp. 7398–7410, Sep. 2018, doi: 10.1109/TPEL.2017.2766605.

[17] W. Zhong and S. Y. Hui, "Reconfigurable wireless power transfer systems with high energy efficiency over wide load range," *IEEE Trans. Power Electron.*, vol. 33, no. 7, pp. 6379–6390, Jul. 2018.
[18] W. X. Zhong and S. Y. R. Hui, "Maximum energy efficiency tracking for wireless power transfer systems," *IEEE Trans. Power Electron.*, vol. 30, no. 7, pp. 4025–4034, Jul. 2015.
[19] M. Fu, C. Ma, and X. Zhu, "A cascaded boost-buck converter for high efficiency wireless power transfer systems," *IEEE Trans. Ind. Inform.*, vol. 10, no. 3, pp. 1972–1980, Aug. 2014.
[20] M. Fu, H. Yin, X. Zhu, and C. Ma, "Analysis and tracking of optimal load in wireless power transfer systems," *IEEE Trans. Power Electron.*, vol. 30, no. 7, pp. 3952–3963, Jul. 2015.
[21] H. Li, J. Li, K. Wang, W. Chen, and X. Yang, "A maximum efficiency point tracking control scheme for wireless power transfer systems using magnetic resonant coupling," *IEEE Trans. Power Electron.*, vol. 30, no. 7, pp. 3998–4008, Jul. 2015.
[22] T. D. Yeo, D. Kwon, S. T. Khang, and J. W. Yu, "Design of maximum efficiency tracking control scheme for closed-loop wireless power charging system employing series resonant tank," *IEEE Trans. Power Electron.*, vol. 32, no. 1, pp. 471–478, Jan. 2017.
[23] Z. Huang, S. C. Wong, and C. K. Tse, "Control design for optimizing efficiency in inductive power transfer systems," *IEEE Trans. Power Electron.*, vol. 33, no. 5, pp. 4523–4534, May 2018.
[24] T. Diekhans and R. W. de Doncker, "A dual-side controlled inductive power transfer system optimized for large coupling factor variations and partial load," *IEEE Trans. Power Electron.*, vol. 30, no. 11, pp. 6320–6328, Nov. 2015.
[25] Z. Li, K. Song, J. Jiang, and C. Zhu, "Constant current charging and maximum efficiency tracking control scheme for supercapacitor wireless charging," *IEEE Trans. Power Electron.*, vol. 33, no. 10, pp. 9088–9100, Oct. 2018, doi: 10.1109/TPEL.2018.2793312.
[26] Q. Chen, L. Jiang, J. Hou, X. Ren, and X. Ruan, "Research on bidirectional contactless resonant converter for energy charging between EVs," in *Proc. IEEE 39th Annu. Conf. Ind. Electron. Soc.*, Vienna, Austria, Nov. 2013, pp. 1236–1241.
[27] K. Colak, E. Asa, M. Bojarski, D. Czarkowski, and O. C. Onar, "A novel phase-shift control of semibridgeless active rectifier for wireless power transfer," *IEEE Trans. Power Electron.*, vol. 30, no. 11, pp. 6288–6297, Nov. 2015.
[28] X. Qu, W. Zhang, S. C. Wong, and C. K. Tse, "Design of a current-source-output inductive power transfer LED lighting system," *IEEE J. Emerg. Sel. Topics Power Electron.*, vol. 3, no. 1, pp. 306–314, Mar. 2015.
[29] M. Budhia, J. T. Boys, G. A. Covic, and C. Y. Huang, "Development of a single-sided flux magnetic coupler for electric vehicle IPT charging systems," *IEEE Trans. Power Electron.*, vol. 60, no. 1, pp. 318–328, Jan. 2013.
[30] Popular Science, "Tesla car can be summoned and park itself," 2016. [Online]. Available: https://www.popsci.com/creeping-toward-kitt-now-tesla-can-be-summoned-and-park-itself-video
[31] J. Yin, D. Lin, T. Parisini, and S. Y. R. Hui, "Front-end monitoring of the mutual inductance and load resistance in a series–series compensated wireless power transfer system," *IEEE Trans. Power Electron.*, vol. 31, no. 10, pp. 7339–7352, Oct. 2016.

Zhicong Huang (M'18) received the B.Eng. degree in electrical engineering and automation and the M.Phil. degree in mechanical and electronic engineering from the Huazhong University of Science and Technology, Wuhan, China, in 2010 and 2013, respectively, and the Ph.D. degree in power electronics from The Hong Kong Polytechnic University, Hong Kong, in 2018.

He is currently a Postdoctoral Fellow with the State Key Laboratory of Analog and Mixed-signal VLSI, University of Macau, Macau, China, under the UM Macao Postdoctoral Fellowship of the UM Macao Talent Program. His research interests include power electronics and its applications.

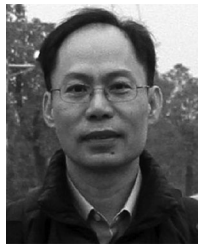

Siu-Chung Wong (M'01–SM'09) received the B.Sc. degree in physics from the University of Hong Kong, Hong Kong, in 1986, the M.Phil. degree in electronics from the Chinese University of Hong Kong, Hong Kong, in 1989, and the Ph.D. degree from the University of Southampton, Southampton, U.K., in 1997.

He is currently an Associate Professor with the Department of Electronic and Information Engineering, The Hong Kong Polytechnic University, Hong Kong. In 2012, he was appointed a Chutian Scholar Chair Professor by the Hubei Provincial Department of Education, China and the appointment was hosted by Wuhan University of Science and Technology, Wuhan, China. In 2013, he was appointed a Guest Professor by the School of Electrical Engineering, Southeast University, Nanjing, China. He was a Visiting Scholar with the Center for Power Electronics Systems, Virginia Tech, VA, USA, in November 2008, with the Aero-Power Sci-Tech Center, Nanjing University of Aeronautics and Astronautics, Nanjing, China, in January 2009, and with the School of Electrical Engineering, Southeast University, Nanjing, China, in March 2012.

Dr. Wong is a member of the Electrical College, The Institution of Engineers, Australia. He is an Associate Editor for the IEEE TRANSACTIONS ON CIRCUITS AND SYSTEMS II, an Editor for the *Energy and Power Engineering Journal,* and a Member of the Editorial Board of the *Journal of Electrical and Control Engineering*.

Chi K. Tse (M'90–SM'97–F'06) received the B.Eng. (Hons.) degree with first-class honors in electrical engineering, and the Ph.D. degree from the University of Melbourne, Melbourne, Vic., Australia, in 1987 and 1991, respectively.

He is presently a Chair Professor with the Hong Kong Polytechnic University, Hong Kong, where he was the Head of the Department of Electronic and Information Engineering from 2005 to 2012. His research interests include power electronics, nonlinear systems and complex network applications.

Prof. Tse was was a recipient of many research and industry awards, including the Prize Paper Awards by the IEEE TRANSACTIONS ON POWER ELECTRONICS in 2001, 2015, and 2017; the Best Paper Award by the *RISP Journal of Signal Processing* in 2014; the Best Paper Award by the International Journal of Circuit Theory and Applications in 2003; two gold medals at the International Inventions Exhibition in Geneva in 2009 and 2013; a silver medal at the International Invention Innovation Competition in Canada in 2016, and many recognitions by the academic and research communities, including honorary professorship by several Chinese and Australian universities, Chang Jiang Scholar Chair Professorship, IEEE Distinguished Lectureship, Distinguished Research Fellowship by the University of Calgary, Gledden Fellowship and International Distinguished Professorship-at-Large by the University of Western Australia. While with the Hong Kong Polytechnic University, he was the recipient of the President's Award for Outstanding Research Performance twice, the Faculty Research Grant Achievement Award twice, the Faculty Best Researcher Award, and several teaching awards. He is and has served as the Editor-in-Chief for the IEEE TRANSACTIONS ON CIRCUITS AND SYSTEMS II (2016–2019), the IEEE CIRCUITS AND SYSTEMS MAGAZINE (2012–2015), and the IEEE CIRCUITS AND SYSTEMS SOCIETY NEWSLETTER (since 2007); an Associate Editor for three IEEE Journal/Transactions; and an Editor for the *International Journal of Circuit Theory and Applications*. He is on the editorial boards of a few other journals. He currently chairs the steering committee for the IEEE TRANSACTIONS ON NETWORK SCIENCE AND ENGINEERING. He is also a Panel Member of Hong Kong Research Grants Council, and a member of several professional and government committees.